LAWRENCE
LIVERMORE
NATIONAL
LABORATORY

UCRL-CONF-217922

Methods for increasing the efficiency of Compton imagers

L. Mihailescu, K. Vetter, M. Burks, D. Chivers, M. Cunningham, D. Gunter, K. E. Nelson

January 3, 2006

IEEE Nuclear Science Symposium
Fajardo, PR, United States
October 22, 2005 through October 29, 2005

Methods for increasing the efficiency of Compton imagers

L. Mihailescu, K. Vetter, M. Burks, D. Chivers, M. Cunningham, D. Gunter, K. E. Nelson

***Abstract*–A Compton scatter camera based on position sensitive, planar Ge and Si(Li) detectors with segmented electrodes is being developed at LLNL. This paper presents various methods that were developed to increase the position resolution of the detectors, the granularity and capability to reconstruct the scattering sequence of the gamma-ray within the detectors. All these methods help to increase the efficiency of the imager, by accepting more photons in the final image. The initial extent and diffusion of charge-carrier clouds inside the semiconductor detectors are found to affect profoundly the fraction of interactions that deposit charge in multiple adjacent electrodes. An accurate identification of these charge-shared interactions is a key factor in correctly reconstructing the position of interactions in the detector.**

I. Introduction

THE introduction of position sensitive semiconductor detectors helped revitalize the Compton scatter camera concept in the last few years. Several Compton camera devices based on CdZnTe, high purity Germanium and Silicon detectors are under development targeting applications in astrophysics, bio-medical research or homeland security. Some of these systems provide images of good resolution, but most have very low efficiency. Only a fraction of the total detected photons contribute to the image. To obtain reasonable resolution, the average distance between the interactions must be large as compared with the position uncertainty of individual interactions, so that only events with widely separated and clean interactions can be used for imaging.

Improved efficiency must be demonstrated for a Compton scatter camera to become a competitive gamma-ray imaging method. The data analysis methods reported in this paper aim to improve imaging efficiency with semiconductor Compton cameras, by increasing the number and accuracy of imageable events. The developed methods were tested on a semiconductor-based Compton camera system developed at the Lawrence Livermore National Laboratory (LLNL). The camera contains double sided segmented Si(Li) and Ge detectors [1], [2] (see Figure 10; details about the device can be found in the paper by Cunninham et al. submitted to this conference).

Manuscript received November 10, 2005. The authors are with the Lawrence Livermore National Laboratory, Livermore, CA, USA.

This work was sponsored by the Office of Research and Development of the Department of Homeland Security. This work was performed under the auspices of the U.S. Department of Energy by University of California, Lawrence Livermore National Laboratory under Contract W-7405-Eng-48.

UCRL-CONF-217922

There are four main factors that affects the imaging efficiency of Compton imagers: the detection *quantum efficiency*, *detection granularity*, *position resolution* and *energy resolution* for each interaction. Improvement in detection quantum efficiency can be obtained by optimizing the detection geometry and scaling up the detection system. This is not the subject of the present work, as it is not the energy resolution. The methods presented here address mainly the position resolution and detection granularity. In the case of most segmented detectors, the position resolution is determined by the detection granularity, alone. However, a superior position resolution can be obtained by using position interpolation methods. The *detection granularity* represents the capability of the system to discriminate multiple interactions occurring in the same detector [3]. A finer detection granularity helps to increase the fraction of detected events whose interactions are correctly identified, by a better differentiation of multiple interactions occurring in close proximity. We introduce in this paper methods able to increase the granularity of the system by discriminating multiple interactions taking place in adjacent segments from single interactions that induce signals in two adjacent segments.

II. Segment Matching and Position Extraction

A. Segment matching

Utilization of events with closely spaced interactions requires maximum position resolution and granularity of the detector. Despite a limited segment pitch size of 2mm, position resolutions in the sub-millimeter range are demonstrated by using new waveform filtering methods. By analyzing the induced signals in adjacent segments, the position of the interaction within the segment width can be inferred [3]. The depth of interaction is determined within 0.5mm by measuring the difference in the arrival time of the electrons and

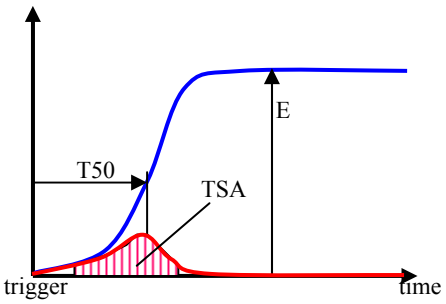

Figure 1 Representation of waveform parameters used for the identification of interactions

holes to the opposite electrodes. The best position resolution achievable with Ge detectors is ultimately limited by the path length of the electrons produced in Compton or photoelectric interactions and the subsequent spread of the charge carriers in the crystal due to diffusion and electrostatic repulsion. The reconstruction of gamma-ray interactions implies the determination of the number of interactions in the active volume of the imager, as well as their energies and three-dimensional positions.

A so-called *Comprehensive Event Selection* algorithm is used to match the information from firing segments in a DSSD. The result of this algorithm is a list of the interactions taking place in the detector for each detected photon. The parameters associated with each interaction are: energy, 3D position, detector identifier (in a system of multiple detectors), and confidence level. For each event consisting of one or more interactions, the algorithm will deliver a figure-of-merit (FoM_CES) labeling the result of the algorithm. A figure-of-merit between 0 and 1 will be attached to accepted events. Its value will be proportional with the confidence level for the event as a whole. A figure-of-merit outside [0, 1] will label an event which has firing segments that can not be properly matched. In this case, the FoM_CES value will code the reason for the mismatch. Such an event is discarded for imaging purposes.

The algorithm uses as input a list of firing segment parameters. The parameters associated to the firing segments are obtained before in the data acquisition system (see Figure 1). For each firing segment, the parameters provided are *E*, *T50*, *R* and *gapTest*, where *E* [keV] is the deposited energy, *T50* [ns] is the time when the pulse reaches 50% of its total amplitude, *R* is the ratio of the transient signal amplitudes (TSA) of the two adjacent segments (described below), and *gapTest* is the parameter indicating the match in the waveform of the signal from the present channel and the signal from a firing adjacent channel, if present (described below).

As electron and hole mobility are similar for Si(Li) and HPGe detectors, we expect an equal number of electrons and holes to be collected on the opposite sides of a DSSD (the AC and DC sides). As a result, the pulse amplitudes will be similar on both sides. In this project, we have arbitrarily decided to use the AC segments to determine the x-coordinate of the interaction, and the DC segments to determine the y-coordinate. Segment matching is thus the process of identifying which AC and DC strips.

The segments are matched according to the proximity in the energy between firing segments on opposite electrodes. The matching process contains several successive steps. A first step of the algorithm attempts to match a single firing segment on one electrode with a single firing segment on the opposite electrode (*1-1 matches*). Afterwards, the remaining firing segments are checked as the sum of energies of any two firing segments on one electrode against one firing segment on the other electrode (*2-1and 1-2 matches*). *1-2*, *2-1* and *2-2* matches are either caused by a single interaction or two interactions. A single interaction may produce signals on two strips on the same side is the interaction occurs in the gap between two strips. If the two firing segments on an electrode are adjacent to each other, a model for a single interaction depositing energy in the two segments (which we term as *charge sharing*) is checked upon. In the third step the higher multiplicity matches are analyzed (the *2-2, 3-2, 2-3, 1-3, 3-1 matches*). In the present implementation, only *1-1*, *1-2*, and *2-1 matches* are accounted for. For each assumed match, a matching likelihood P_{kl} is calculated to include probabilities for each segment firing to contain an interaction consistent with the assumed model (P_k and P_l). A match is adopted if the calculated likelihood is above a certain threshold. For 1-1 matches, the match probability becomes:

$$P_{kl} = \frac{1}{\sigma\sqrt{2\pi}} e^{\frac{-(E_k - E_l)^2}{\sigma^2}} P_k P_l \quad , \qquad (1)$$

In this case, P_k and P_l represent the probability that the firing segments have fired because of a single interaction, as opposed to multiple interactions. E_k and E_l are the energies of the two segments, and σ is the equivalent standard deviation of the measured energies.

For 1-2 or 2-1 matches, if the 2 firing segments on the same electrode are non-adjacent, the assumed model accounts for 2 separate interactions depositing energy in a single segment on one side and in two segments on the other side. The probability for the match becomes:

$$P_{kl,2I} = \frac{1}{\sigma\sqrt{2\pi}} e^{\frac{-(E_k - \sum_{l1,l2} E_{l1,l2})^2}{\sigma^2}} P_{k,2I} P_{(l1,l2),2I} \quad . (2)$$

The term $P_{k,2I}$ accounts for the probability of two interactions inducing the signal in segment *k*. The term $P_{(l1,l2),2I}$ accounts for the probability of one interaction in segment *l1* and one interaction in segment *l2*.

If a single interaction is assumed to produce a charge sharing instance, the probability is defined as:

$$P_{kl,CS} = \frac{1}{\sigma\sqrt{2\pi}} e^{\frac{-(E_k - \sum_{l1,l2} E_{l1,l2})^2}{\sigma^2}} P_k P_{(l1,l2),CS} \quad . \qquad (3)$$

The term $P_{(l1,l2),CS}$ represents the probability for the signal waveforms of two adjacent segments *l1* and *l2* to have been produced by a single interaction in a charge sharing interaction. One alternative to this model is a case of two separate interactions. Such a model is checked upon by equation (2).

If no information exists to support the calculation of the $P_{(l1,l2),CS}$, $P_{(l1,l2),2I}$, P_k and P_l terms, the match is made by simply taking the minimum value for the quadratic difference between the segment energies:

$$\xi_{kl} = \frac{(E_k - E_l)^2}{\sigma^2} \quad . \qquad (4)$$

A match is accepted only if the overall likelihood is above a preset threshold.

III. Identification of Charge-Shared Interactions

A. Charge sharing

Charge sharing is the process by which the charge carriers produced by a single interaction are collected by two adjacent electrodes. It is important to identify such interactions in order to discriminate them from cases when multiple interactions induce signals in adjacent segments. For example, in Figure 2, we see two different 2-1 events – one produced by a single interaction with charge sharing and one by two interactions. It is important to correctly identify which process produced these signals to correctly image the gamma-ray.

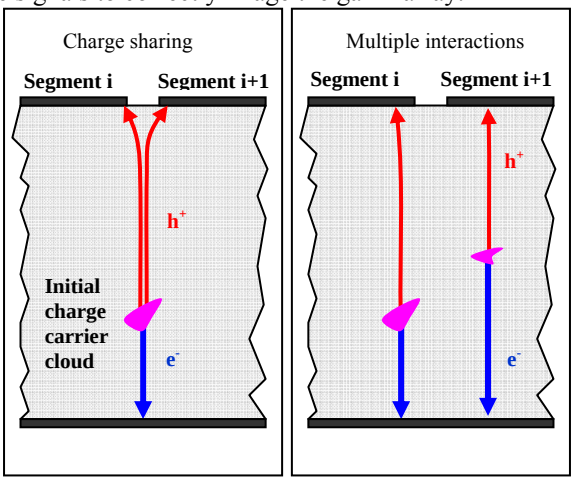

Figure 2 Comparative representation of a single charge shared interaction and a double interaction event.

The predominance of the charge sharing interactions is determined by the extension of their charge carrier clouds. The initial dimensions of these clouds are determined by the path of the Compton-electrons or photoelectrons in the detection material. During the drift toward electrodes, the clouds are further enlarged by the thermal diffusion, electrostatic repulsion between charge carriers, and other inelastic scattering mechanisms inside the crystal lattice.

The diffusion coefficient for electrons and holes $D_{e,h}$ is:

$$D_{e,h} = \frac{k_B T}{e} \mu_{e,h} \quad (5)$$

where k_B is Boltzman's constant, $\mu_{e,h}$ is the electron and hole mobility, T is the temperature of the crystal, e is the electron's charge. The evolution of the charge carrier cloud during their drift towards the electrodes as determined by the diffusion is represented in Figure 3.

If the probability for an interaction to share charges between two electrodes is *p*, the expected fraction of events of *N* interactions that contain a number *n* of charge-shared interactions is found by the binomial distribution:

$$P(n,T) = C_n^T p^n (1-p)^{T-n}, \quad (6)$$

where *p* is the probability for the occurrence of a charge sharing case, C_n^T is the combination of *T* elements taken *n* times, and *T* is the number of trials. In the present case, the number of trials, $T=2N$, where *N* is the number of interactions (each interaction in a DSSD will create two chances for charge sharing, one for the AC segments, one for DC segments). The probability for at least a charge sharing case in an *N* interaction event is the sum of all probabilities that 1, 2,…, 2*N* charge sharing cases will occur:

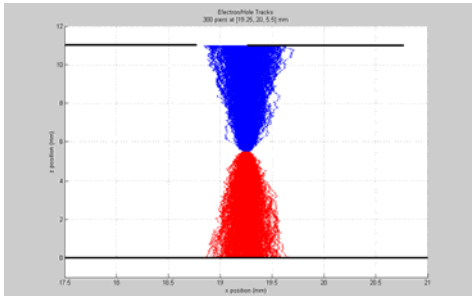

Figure 3 Simulated trajectories of charge carriers in a planar detector following a gamma-ray interaction. Thermal diffusion was accounted for.

$$P(n \geq 1,2N) = P(1,2N) + P(2,2N) + \ldots = 1 - P(0,2N) \quad (7)$$

That is:

$$P = 1 - (1-p)^{2N}$$

Examples: p=15%, N=3; P=62%
p=20%, N=4; P=83%

This high probability for at least a charge sharing instance in any given event suggests that charge sharing is a very important factor in the event selection process, and needs to be accounted for.

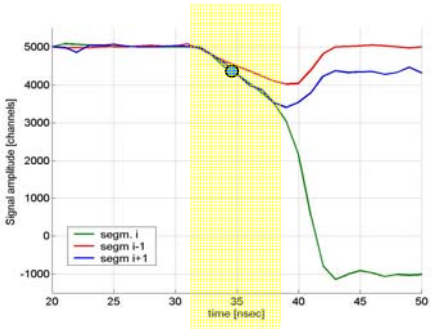

Figure 4 Example of signal waveforms produced by a charge sharing interaction. The yellow shaded time interval represents the gap-test interval.

The signals induced by a charge sharing interaction in the two adjacent segments have the same shape within a certain time interval. This is a significant feature that is used to discriminate such interactions. The similarity of shapes can be explained by the fact that at the border between two segments, the charge cloud path goes through similar weighting fields associated with the two segments. An example of induced signals is shown in Figure 4.

B. Gap test version 1

Candidates for charge sharing interactions are the (2-1) trigger patterns, with the two adjacent firing segments on one side. For such cases, it is hypothesized that the case is a charge sharing interaction. A Chi square hypothesis test is used to check this hypothesis.

$$\chi^2 = \frac{\sum_{i=sl}^{sr}(s_{1i} - m_i)^2}{\sigma_{S_{1i}}^2} + \frac{\sum_{i=sl}^{sr}(s_{2i} - m_i)^2}{\sigma_{S_{2i}}^2}, \quad (8)$$

where s_{1i} is the sample amplitude of the first waveform, s_{2i} is the sample amplitude of the second waveform, $\sigma_{S_{1i}}$ and $\sigma_{S_{2i}}$ are the sample standard deviations for the first waveform, and the second waveform, respectively. The sums run over a waveform segment starting with sample index *sl* and ending with the sample index *sr* as determined in respect to the sample closest to the point where the leading edge passes a low level threshold. m_i is a model for the sample of index *i*. For a charge shared event, we expect to have identical signal waveforms within the specified time interval. The model m_i we choose is the average of the two waveforms:

$$m_i = \frac{s_{1i} + s_{2i}}{2}. \quad (9)$$

If the sample standard deviation is the same for all samples of the two waveforms, then

$$\sigma_{S_{1i}} = \sigma_{S_{2i}} = \sigma. \quad (10)$$

The estimation of the sample standard deviation is done using a region of the signal that does not contain pulses, but only noise:

$$\sigma = \sqrt{\frac{1}{N}\sum_{i=1}^{N}(s_i - \bar{s})^2}. \quad (11)$$

As a result, the gap test based on the Chi square test becomes:

$$gapTest = \frac{\sum_{i=sl}^{sr}(s_{1i} - s_{2i})^2}{\sigma^2}. \quad (12)$$

If the hypothesis is correct (i.e., the signals are from a single sharge-shared interaction), the variation in the s_{ji} samples is expected to follow a normal distribution. Thus, the *gapTest* distribution will be a chi-square distribution. For a certain significance level, α, to accept the hypothesis, an upper threshold for *gapTest* will be chosen from the critical value of the Chi square distribution:

$$gapTest < x_\alpha(\chi_N^2), \quad (13)$$

here N is the number of degrees of freedom.

As described below, this first version of a gap test has been tested with experimental data and found to identify only a part of charge-shared events.

C. Gap test version 2

As described above, waveforms have similar shape when the charge carriers drift relatively far from the collecting electrode. As a result, the first version of our gap test algorithm produced good results for interactions taking place far from the collecting electrodes, but could not identify the charge shared interactions taking place close to the electrodes (see Figures 5 and 6). When the interaction takes place near the collecting segments, the signal waveforms from the two strips are very different from each other in the signal window used by the first version of the algorithm. In such a case, the waveforms will have a similar shape only toward the tail of the pulse leading edge, and then, there will be an off-set in amplitude determined by the difference in the pulse amplitudes of the two segments.

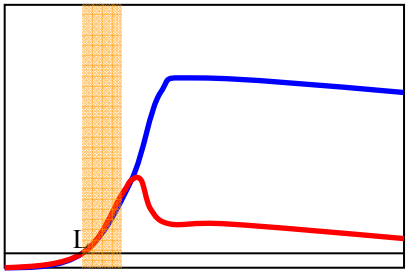

Figure 5 Signals induced in a charge sharing interaction taking place away from the collecting electrode

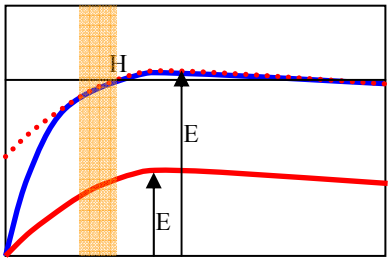

Figure 6 Signals induced in a charge sharing interaction taking place close to the collecting electrode

In order to identify near-electrode charge sharing interactions, the position of the window will be moved, and a correction has to be made for the difference in the amplitude between the two waveforms (see Figure 6). Therefore, a two-step test is needed to identify both types of charge sharing interactions.

Another change in the *gaptest* formula as compared with the first algorithm is the introduction of a $kE_{\max}$ term. This term will relax the assumed standard deviation σ so that, in the case when the waveforms signal to noise ratio is large (as it will be at high energies), the relatively small differences between the two waveforms due to the slightly different weighting fields associated with the two segments will not be reflected in the chi-squared test. With this modification, the first step in the gap test (to identify charge sharing interactions far away from the collecting electrode is:

$$gapTest1 = \frac{\sum_{i=L}^{L+W}(S_{1i} - S_{2i})^2}{\sigma^2 + (kE_{\max})^2}. \quad (14)$$

and is applied to the time window shown in Figure 5, which starts when the pulse amplitudes exceed a low-level threshold L (typically set at 3 times σ to avoid triggering this test on noise).

The second step in the gap test (to identify near-electrode charge sharing interactions) must include a correction for the pulse amplitudes *E1* and *E2*, and thus is:

$$gapTest2 = \frac{\sum_{i=H-W}^{H}(S_{1i} - S_{2i} + E_2 - E_1)^2}{\sigma^2 + (kE_{\max})^2}. \quad (15)$$

where the time window is shown in Figure 6 and ends when one of the pulses exceeds an upper-level threshold H, typically 3 to 4 times σ below the total pulse amplitude.

By selecting the minimum of these two values:

$$gapTest = \min(gapTest1, gapTest2) \quad (16)$$

we can apply the same hypothesis test as was discussed for the version 1 of the gap test (equation (23)).

D. Gap test experimental results

We have used a DSSD planar Ge detector to check the gap test algorithm. The detector has a circular shape with a diameter of 100mm. The detector active area covers a square-like shape with rounded corners. The dimension of the active area is 76 mm from side to side. The detector has a thickness of 11mm with guard-rings around each electrode of variable thicknesses between 2.3 to 5.9 mm. The 38 segments on each electrode have a pitch size of 2 mm, with a 0.5 mm gap between each other. The bias voltage used was 1000V.

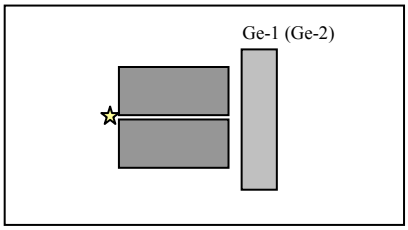

Figure 7 The experimental setup with a circular 1mm hevimet collimator in front of a Ge detector.

The experimental system consisted of one of detector, a Cs-137 source, and a 1mm diameter pinhole collimator interposed between the source and the detector (see Figure 7). The collimator was aligned to irradiate the detector in the middle of a pair of AC and DC segments and on the border between segments.

The results are graphically shown in 5 and 6. For firing adjacent segments, a chi-squared distribution is expected to be formed by the *gapTest* values of charge shared interactions. However, the first version of the gap test algorithm shows that many of the 1-2 and 2-1 events can be found outside the chi square distribution. These are the events that are not recognized by the test to have similar waveforms, which would indicate the presence of multiple interactions. However, there is a very big difference in these numbers when moving the irradiation spot from the middle of the segment to the gap between two segments. Monte Carlo simulations would suggest only a 7% increase in the multiplicity of 1-2 events when changing the irradiation spot from the middle of the segment into the gap, whereas the experimental results show a factor of 2 increase. Clearly, this test is not complete, failing to recognize some of the charge sharing interactions.

The gap test version 2, by comparison with the first version, provides much more consistent results. The difference between the numbers of 1-2 events outside the chi square distribution varies by a factor of 20%, between the two irradiation points, much closer to the 7% expected from Monte Carlo simulations. Higher amplitudes have been obtained for the chi square distribution when the irradiation of the detector takes place in the gap between segments, than in the middle of the segment. This is in agreement with a higher charge sharing probability when the interactions take place in close proximity to the gap between segments.

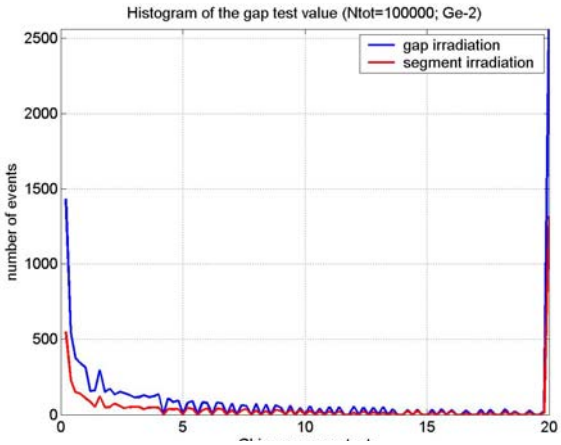

Figure 8 Histogram of *gapTest* values using gap test version 1

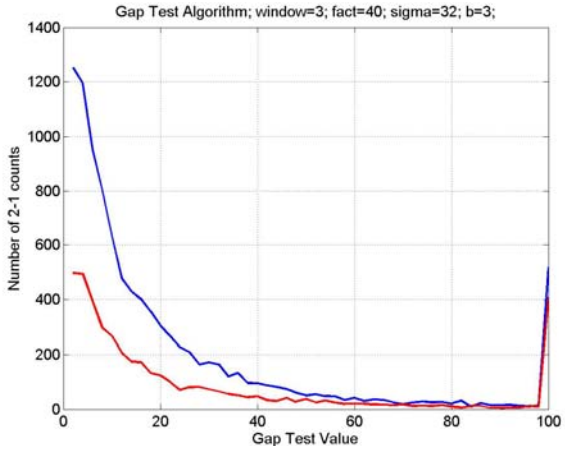

Figure 9 Histogram of *gapTest* values using gap test version 2

E. Imaging efficiency results

The influence of using the proposed segment matching and gap test algorithms on Compton imaging sensitivity has been investigated. We have used a detection system of two DSSD detectors: a planar Si(Li) detector and the Ge detector discussed above. The Si(Li) detector had 32 strips of 2mm pitch size on each side. The detector thickness is 10mm. The relative position of the two detectors is shown in Figure 10. An event is collected only if there is coincidence between the two detectors. Figures 11 and 12 show the fraction of events that are kept after matching the firing segments (blue bars), after determining the scattering sequence of the matched events (green bars), and after event back-projection (red bars), as function of the number of identified interactions. The total number of coincident events is normalized to 1. Figure 11 shows the results for using a simple strip matching algorithm

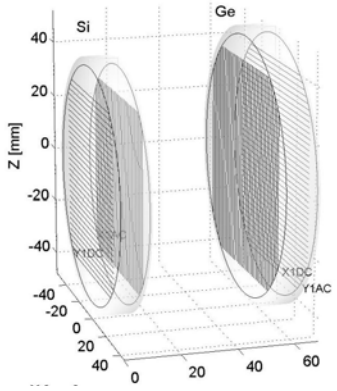

Figure 10 Si(Li)-Ge Compton camera imaging assembly

that only considers *(1-1)* matches. In this case, a total imaging efficiency of 12% is obtained. The imaging efficiency is calculated as the fraction of the events that are imaged out of the total number of events from the photopeak that produce interactions in both detectors. Figure 12 shows the results of using the algorithms proposed in this paper. A total imaging of 37% is obtained, which is a 3 times increase in efficiency as compared with the simple strip matching approach.

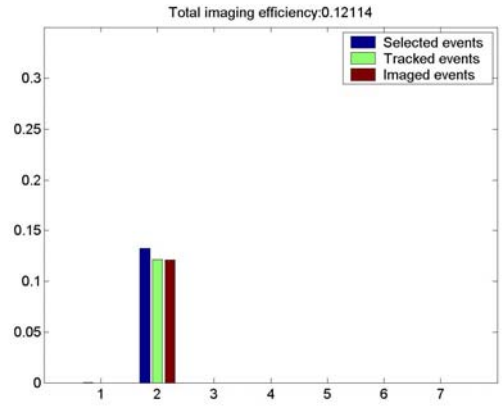

Figure 11 Efficiency for simple segment matching of (1-1) trigger events (blue bars), event tracking (green bars), and imaging (red bars), as function of identified number of interactions

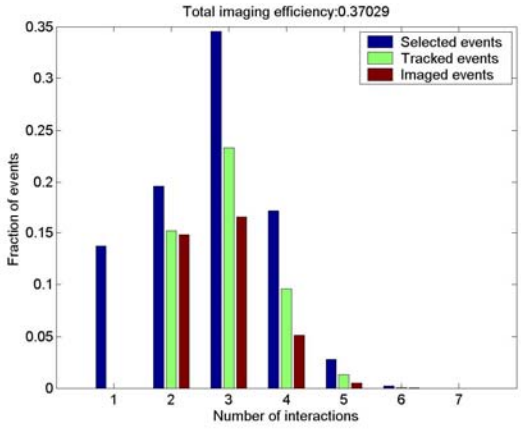

Figure 12 Efficiency for segment matching using the algorithm described in this work (blue bars), event tracking (green bars), and imaging (red bars), as function of the identified number of interactions

IV. Conclusions

We have proposed and demonstrated methods that will help improve the resolution and sensitivity of Compton imagers using large double-sided segmented semiconductor detectors. The method aimed at improving detection granularity by identifying charge shared interactions has been shown to provide consistent results. However, a more quantitative assessment of these methods will be pursued.

Acknowledgment

We would like to thank Davor Protic and Ethan Hull for providing us the detectors. This work was funded by the Department of Homeland Security. This work was performed under the auspices of the U.S. Department of Energy by University of California, Lawrence Livermore National Laboratory under Contract W-7405-Eng-48.

References

[1] M. Amman, P.N. Luke, ``Three-dimensional position sensing and field shaping in orthogonal-strip germanium gamma-ray detectors", Nucl. Instr. Meth. A, 452 (1-2), pp.155-166, 2000;

[2] Hull, E.L. et al., SPIE Proceedings,Bellingham Washington, 4507, 2001.

[3] L. Mihailescu, K.M. Vetter, M.T. Burks, E.L. Hull, W.W. Craig, "SPEIR: a Ge Compton camera" NIM-A , accepted for publication 2005

[4] K. Vetter, M. Burks and L. Mihailescu, *Nucl. Instr. Meth. Phys. Res. A* **525** (2004), p. 322